Sensors and Materials, Vol. 38, No. 5 (2026) 2681–2692
MYU Tokyo

S & M 4462

Speed Estimation Stator-field-orientation-controlled Induction Motor Drive with Resistance Parameter Identification

Yung-Chang Luo,* Ruei-Chi Shiu, Wen-Cheng Pu, and Hao-You Huang

Department of Electrical Engineering, National Chin-Yi University of Technology,
No. 57, Sec. 2, Zhongshan Rd, Taiping Dist, Taichung 41170, Taiwan (ROC)

(Received December 19, 2025; accepted April 22, 2026)

Keywords: stator-field-orientation-controlled (SFOC), speed estimation, model reference adaptive control (MRAC), stator resistance parameter identification, fixed trace algorithm (FTA)

A stator resistance parameter identification was proposed for the speed estimation stator-field-orientation-controlled (SFOC) induction motor (IM) drive. The decoupled SFOC IM drive was formulated on the basis of stator current and flux to achieve maximum torque-per-ampere control, with the stator currents measured using Hall-effect current sensors. An adaptive speed estimation approach based on model reference adaptive control (MRAC) was developed by utilizing the motor's reactive power. To address resistance variations induced by temperature changes, an online stator resistance identification method employing the fixed trace algorithm (FTA) was integrated into the SFOC IM drive. The complete simulation model was implemented using the MATLAB®/Simulink environment, and the control algorithms were realized on a TI DSP 6713-and-F2812 platform to validate the proposed method. Both simulation and experimental results confirmed the effectiveness of the proposed approach.

1. Introduction

Induction motors (IMs) offer several advantages, including a simple structure, low cost, high reliability, strong durability, excellent operational performance, standardized designs across with a wide power range, and seamless integration with variable-frequency drives. Owing to these characteristics, IMs have been widely adopted in modern industrial applications such as smart manufacturing, intelligent building systems, smart agriculture, intelligent transportation, and electric vehicles. However, the mathematical model of an IM is inherently complex, making precise control challenging. By applying field orientation control (FOC) techniques—analogous to the control strategy used in separately excited DC motors—an independent regulation of torque and flux can be achieved. According to FOC theory,[(1)] coordinate transformation enables the decomposition of the IM model into orthogonal flux-current and torque-current components, thereby facilitating maximum torque-per-ampere control.

The implementation of a conventional FOC IM drive typically requires a resolver or an encoder to detect the rotor position; however, the use of these sensors may degrade drive

*Corresponding author: e-mail: luoyc@ncut.edu.tw
https://doi.org/10.18494/SAM6132

ISSN 0914-4935

performance. Several speed estimation methods for FOC IM drives have been reported in the literature, including approaches based on back electromotive force (EMF),[2–5] reduced-order observers,[6–9] sliding-mode observers,[10–12] and fuzzy-logic-based speed regulation.[13–15] Moreover, the realization of an FOC IM drive requires accurate motor parameters. Among these parameters, stator resistance varies significantly with operating temperature, and the variation becomes more pronounced under prolonged heavy-load conditions. When the resistance parameter used in the drive controller deviates from the actual motor resistance, drive performance deteriorates. Therefore, the development of online stator resistance identification techniques for FOC IM drives is essential. Numerous resistance identification methods have been proposed, including estimation based on adaptive control theory,[16–18] inverse-model-based parameter identification,[19,20] extended Kalman filtering,[21–23] and flux-observer-derived resistance adaptation.[24–26] In this study, a decoupled stator-field-orientation-controlled (SFOC) IM drive system based on stator current and flux was established. The three-phase stator currents of the IM were measured using electromagnetic Hall effect current sensors. On the basis of the linear control design of the speed, flux, and two-axis stator current control loops, a systematic controller parameter design method was formulated using root locus and Bode plot techniques. In addition, a model reference adaptive control (MRAC) speed estimation scheme based on motor reactive power was developed. A fixed trace algorithm (FTA) for the online adaptation of stator resistance was also implemented to mitigate the effects of temperature-induced resistance variations.

This paper is organized into six sections. In Sect. 1, we present the research background, motivation, and a review of speed estimation methods for FOC IM drives. In Sect. 2, we describe the development of the decoupled SFOC IM drive system and provide a detailed discussion of the systematic controller parameter design for the two-axis stator current, flux, and speed control loops based on root locus and Bode plot techniques. The speed estimation scheme derived from MRAC theory is presented in Sect. 3. In Sect. 4, we develop a stator resistance parameter identification method using the FTA. In Sects. 5 and 6, we present the simulation and experimental results, respectively, followed by conclusions.

2. Decoupled SFOC IM Drive

The stator and rotor voltage equations of an IM, formulated using stator current and flux as state variables, are given in the synchronous reference frame by[27]

$$R_s \vec{i}_s^{\,e} + (j\omega_e + p)\vec{\lambda}_s^{\,e} = \vec{v}_s^{\,e}, \tag{1}$$

$$\frac{X_r}{X_m}\left[\frac{1}{\tau_r} + \left(j\omega_{sl} + p\right)\right]\vec{\lambda}_s^{\,e} - \frac{X_r}{X_m}\left[R_r + \frac{\sigma X_r}{\omega_b}\left(j\omega_{sl} + p\right)\right]\vec{i}_s^{\,e} = 0, \tag{2}$$

where j denotes the imaginary unit, $p = d/dt$ is the differential operator, and $\vec{i}_s^{\,e} = i_{ds}^e + j i_{qs}^e$, $\vec{v}_s^{\,e} = v_{ds}^e + j v_{qs}^e$, and $\vec{\lambda}_s^{\,e} = \lambda_{ds}^e + j\lambda_{qs}^e$ are the stator current, voltage, and flux, respectively. R_s and

R_r are the stator and rotor resistances, and X_s and X_r are the stator and rotor reactances, respectively, X_m is the mutual reactance between the stator and the rotor, and $\sigma = (1 - X_m^2 / (X_s X_r))$ is the leakage coefficient. $\tau_r = X_r / (\omega_b R_r)$ is the rotor time constant, ω_b is the base speed, ω_r is the electrical speed of the rotor, ω_e is the speed of the synchronous reference coordinate frame, and $\omega_{sl} = \omega_e - \omega_r$ is the slip speed.

Under the SFOC condition ($\lambda_{qs}^e = 0$), the estimated slip speed and *d*-axis stator flux can be derived from Eq. (2) as

$$\hat{\omega}_{sl} = \frac{(1 + \sigma\tau_r s)(X_s / \omega_b) i_{qs}^e}{\tau_r (\hat{\lambda}_{ds}^e - \sigma (X_s / \omega_b) i_{ds}^e)}, \tag{3}$$

$$\hat{\lambda}_{ds}^e = \frac{(1 + \sigma\tau_r s)(X_s / \omega_b)}{1 + \tau_r s} i_{ds}^e - \frac{\sigma\tau_r \hat{\omega}_{sl} (X_s / \omega_b)}{1 + \tau_r s} i_{qs}^e, \tag{4}$$

where s is the Laplace operator and the symbol ^ denotes the estimated value. The *d*-axis stator flux feedforward compensation is defined as

$$i_{dq}^e = \frac{\sigma\tau_r \hat{\omega}_{sl} (X_s / \omega_b)}{1 + \tau_r s} i_{qs}^e. \tag{5}$$

On the basis of Eq. (4), the linear relationship between the estimated *d*-axis stator flux and the *d*-axis stator current is expressed as

$$\hat{\lambda}_{ds}^e = \frac{(1 + \sigma\tau_r s)(X_s / \omega_b)}{1 + \tau_r s} i_{ds}^e. \tag{6}$$

The developed electromagnetic torque under the SFOC condition is derived as

$$T_e = \frac{3P}{4} \cdot i_{qs}^e \hat{\lambda}_{ds}^e, \tag{7}$$

where P is the number of motor poles. Since i_{qs}^e and $\hat{\lambda}_{ds}^e$ are orthogonal and can be independently controlled, the maximum torque-per-ampere control can be achieved. The mechanical equation of an IM is given by

$$T_e = T_L + B_m \omega_{rm} + J_m p \omega_{rm}, \tag{8}$$

where T_L is the load torque, B_m is the viscous friction coefficient, J_m is the motor inertia, and $\omega_{rm} = (2/P)\omega_r$ is the mechanical speed of the motor rotor shaft.

Under the SFOC condition, the *d*-axis and *q*-axis stator voltages can be derived from Eq. (1) and are given respectively by

$$v_{ds}^{e} = R_s i_{ds}^{e} + p\hat{\lambda}_{ds}^{e}, \tag{9}$$

$$v_{qs}^{e} = R_s i_{qs}^{e} + \omega_e \hat{\lambda}_{ds}^{e}. \tag{10}$$

The second term on the right side of Eq. (10) shows a coupling component related to $\hat{\lambda}_{ds}^{e}$. By defining the *q*-axis stator voltage feedforward compensation as $\omega_e \hat{\lambda}_{ds}^{e}$, a linear *q*-axis stator voltage equation can be obtained.

On the basis of Eqs. (9) and (6), the plant model of the *d*-axis stator current control loop is derived as

$$G_{P\_i_{ds}} \equiv \frac{i_{ds}^{e}}{v_{ds}^{e'}} = \frac{\omega_b(1+\tau_r s)}{\omega_b R_s + (X_s + \omega_b \sigma\tau_r)s + \sigma\tau_r X_s s^2}. \tag{11}$$

By applying the linearized *q*-axis stator voltage equation derived from Eq. (10), the plant model of the *q*-axis stator current control loop is derived as

$$G_{P\_i_{qs}} \equiv \frac{i_{qs}^{e}}{v_{qs}^{e'}} = \frac{1}{R_s}. \tag{12}$$

According to Eq. (6), the plant model of the flux control loop is derived as

$$G_{P\_\lambda_{dr}} \equiv \frac{\hat{\lambda}_{ds}^{e}}{i_{ds}^{e}} = \frac{(1+\sigma\tau_r s)(X_s/\omega_b)}{1+\tau_r s}. \tag{13}$$

By defining $\Delta T_e = T_e - T_L$, the plant model of the speed control loop is derived from Eq. (8) as

$$G_{P\_\omega_{rm}} \equiv \frac{\omega_{rm}}{\Delta T_e} = \frac{1/J_m}{s + B_m/J_m}. \tag{14}$$

Figure 1 illustrates the decoupled control block diagram of the SFOC IM. In this diagram, (K_{ps}, K_{is}), (K_{pd}, K_{id}), (K_{pf}, K_{if}), and (K_{pq}, K_{iq}) represent the proportional–integral gain pairs of the speed, flux, and *d*-axis and *q*-axis stator current controllers, respectively. The four controllers were designed on the basis of root locus and Bode plot techniques. Because the bandwidths of the internal *q*-axis and *d*-axis stator current control loops are individually significantly higher than those of the outer speed and flux control loops, Eqs. (14) and (13) were used as the controlled plant models for the speed and flux loops, respectively.

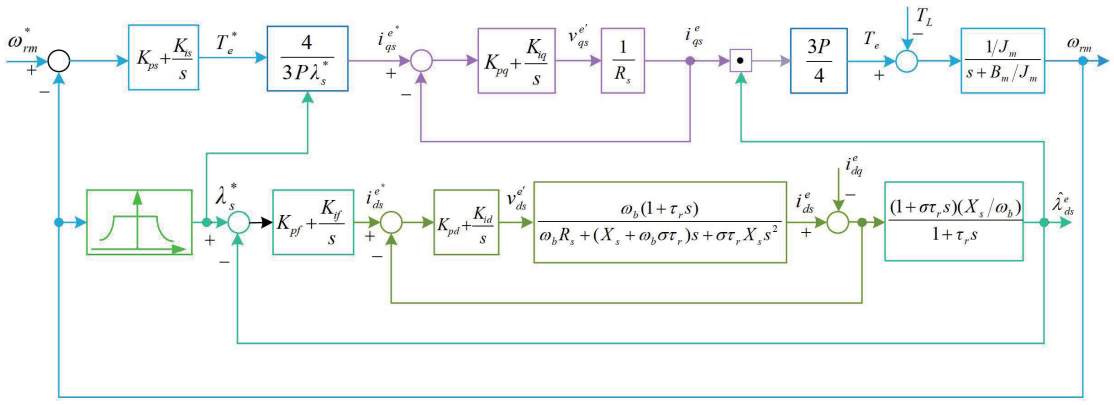

Fig. 1. (Color online) Decoupled control block diagram of the SFOC IM drive.

3. MRAC Speed Estimation Scheme

In the speed estimation SFOC IM drive, the estimated speed signal is used in place of the feedback speed employed in a conventional SFOC IM drive. In this study, the MRAC speed estimation scheme was proposed using the reactive power of the IM.

The reactive power of an IM obtained from the power source is given by

$$Q \equiv \mathrm{Im}(\vec{v}_s^e(\vec{i}_s^e)^*) = v_{qs}^e i_{ds}^e - v_{ds}^e i_{qs}^e, \tag{15}$$

where Im denotes the imaginary part and the symbol * represents the complex conjugate. By substituting Eqs. (9) and (10) into Eq. (15), the reactive power of an IM under the SFOC condition is obtained as

$$Q' = i_{ds}^e \hat{\lambda}_{ds}^e \hat{\omega}_e - i_{qs}^e s\lambda_{ds}^e. \tag{16}$$

According to the MRAC theory,[28] Eq. (15) is selected as the reference model, as it does not include the estimated variable $\hat{\omega}_e$, whereas Eq. (16), which contains $\hat{\omega}_e$, is chosen as the adjustable model. The difference between the outputs of the two models is then processed by an adaptation mechanism to adjust $\hat{\omega}_e$, and the estimated synchronous position angle $\hat{\theta}_e$ is obtained by integrating $\hat{\omega}_e$ using an integrator 1/s. Moreover, the estimated rotor speed is given by $\hat{\omega}_r = \omega_e - \omega_{sl}$. The proposed MRAC speed estimation scheme is illustrated in Fig. 2.

4. Stator Resistance Parameter Identification Using FTA

An FTA was developed for the online identification of the stator resistance parameter to compensate for resistance variations caused by temperature changes, thereby enhancing the performance of the SFOC IM drive.

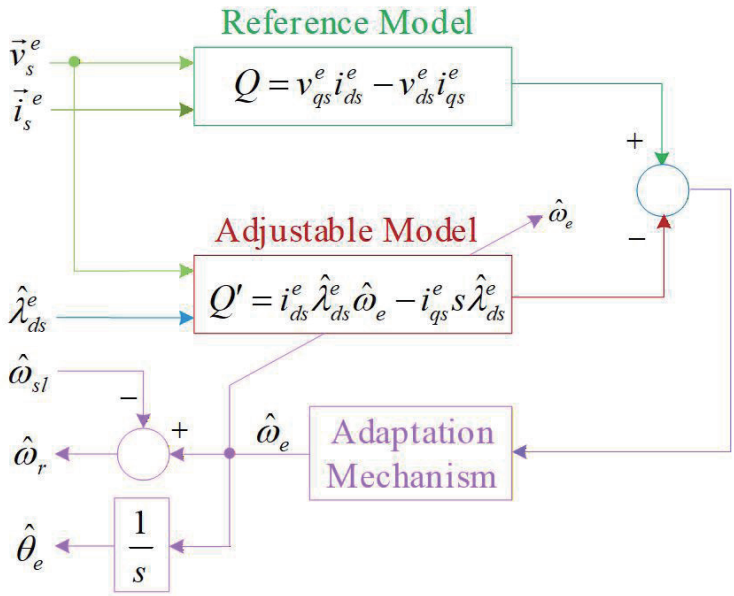

Fig. 2. (Color online) MRAC speed estimation scheme.

The *d*-axis and *q*-axis stator voltage equations are given by Eq. (1) as

$$p\lambda_{ds}^e = v_{ds}^e - R_s i_{ds}^e + \omega_e \lambda_{qs}^e , \tag{17}$$

$$p\lambda_{qs}^e = v_{qs}^e - R_s i_{qs}^e - \omega_e \lambda_{ds}^e . \tag{18}$$

The speed of the synchronous reference frame can be obtained from Eq. (18) as

$$\omega_e = (v_{qs}^e - R_s i_{qs}^e - s\lambda_{qs}^e) / \lambda_{ds}^e . \tag{19}$$

On the basis of Eq. (19), Eq. (17) can be rewritten as

$$p\lambda_{ds}^e = v_{ds}^e - R_s i_{ds}^e + ((v_{qs}^e - R_s i_{qs}^e - s\lambda_{qs}^e) / \lambda_{ds}^e)\lambda_{qs}^e . \tag{20}$$

The stator resistance parameter to be identified can be derived from Eq. (20) as

$$\hat{R}_s = ((v_{ds}^e \lambda_{ds}^e + v_{qs}^e \lambda_{qs}^e - (\lambda_{ds}^e s\lambda_{ds}^e + \lambda_{qs}^e s\lambda_{qs}^e)) / (i_{ds}^e \lambda_{ds}^e + i_{qs}^e \lambda_{qs}^e) . \tag{21}$$

The FTA is an evolution of the recursive least squares (RLS) algorithm and is capable of preventing divergence in the estimation process caused by the denominator approaching zero. In

the conventional RLS algorithm, a fixed forgetting factor is employed; however, in the FTA, the forgetting factor is dynamically adjusted according to the estimation results. This adaptive mechanism enhances the robustness of the FTA against external noise.[29] On the basis of the FTA, the stator resistance parameter identification in Eq. (21) can be derived as

$$\hat{R}_r[N] = \hat{R}_r[N-1] - ((\gamma a[N]) / (1+\gamma(a[N])^2))(R_r[N-1]a[N] - b[N]), \tag{22}$$

where $a[N] = i^e_{ds}\lambda^e_{ds} + i^e_{qs}\lambda^e_{qs}$, $b[N] = (v^e_{ds}\lambda^e_{ds} + v^e_{qs}\lambda^e_{qs} - (\lambda^e_{ds}s\lambda^e_{ds} + \lambda^e_{qs}s\lambda^e_{qs})$, and γ is the gain factor. Figure 3 illustrates the FTA process for online stator resistance parameter identification. R_{sm} and R_{rm} represent the nominal values of the stator and rotor resistances, respectively, and Z^{-1} denotes a unit delay. The identified rotor resistance parameter $\hat{R}_r$ is then incorporated into the SFOC IM drive to compensate for the temperature-induced variations in motor resistance.

Figure 4 illustrates the block diagram of the proposed MRAC speed estimation SFOC IM drive integrated with FTA stator resistance parameter identification. The system comprises a speed controller, a flux controller, and *d*-axis and *q*-axis stator current controllers; *d*-axis stator flux and *q*-axis stator voltage feedforward compensations; estimated slip speed and $i^{e^*}_{qs}$ calculations; coordinate transformation between the three-phase reference frame and the two-axis synchronous reference frame ($2^e \Leftarrow 3$, $2^e \Rightarrow 3$); MRAC rotor speed estimation; and FTA stator resistance parameter identification. In this configuration, the speed controller, flux controller, as well as the *d*-axis and *q*-axis stator current controllers were designed using root locus and Bode plot techniques. The adaptive estimation of rotor speed was implemented according to MRAC theory, while online compensation for temperature-dependent variations in stator resistance was achieved via the FTA scheme. Furthermore, the three-phase stator currents (i_{as}, i_{bs}, and i_{cs}) of the IM were measured using electromagnetic Hall effect current sensors.

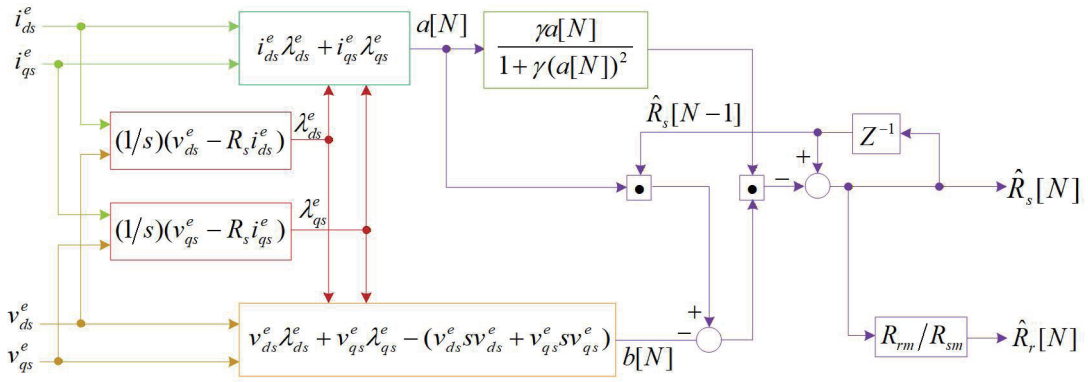

Fig. 3. (Color online) FTA stator resistance parameter identification.

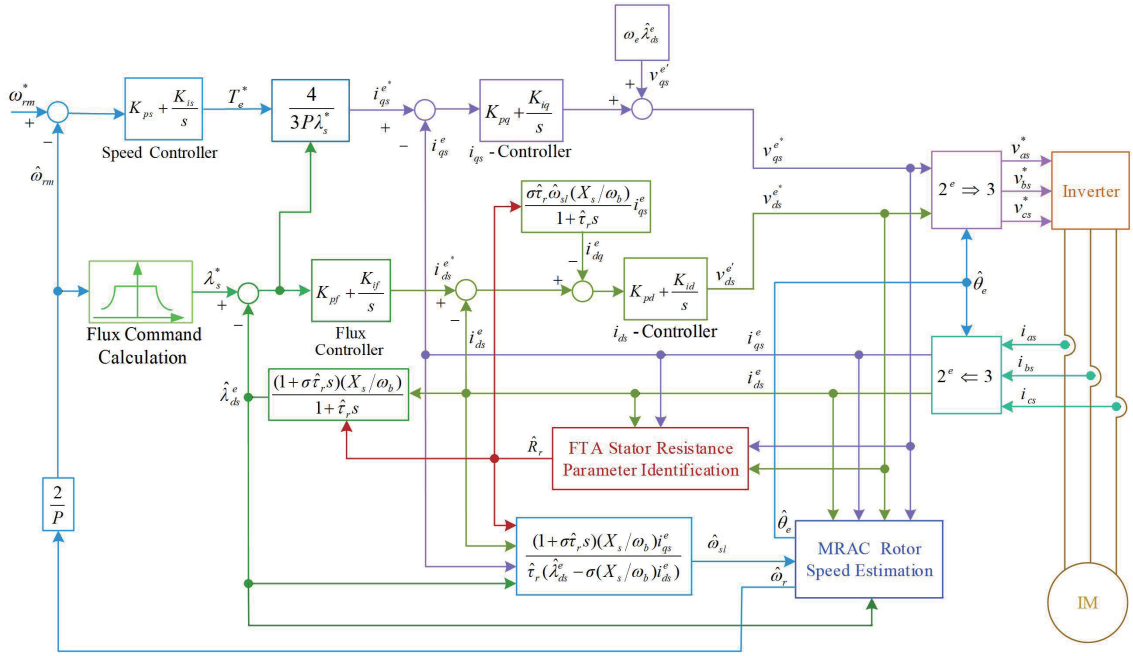

Fig. 4. (Color online) MRAC speed estimation SFOC IM drive with FTA stator resistance parameter identification.

5. Simulation Setup and Results

A three-phase, 220 V, 0.75 kW, Y-connected IM was used as the controlled plant in the experiments to validate the effectiveness of the proposed MRAC speed estimation SFOC IM drive with FTA stator resistance parameter identification. In a running cycle, the speed command was designed as follows: forward acceleration from $t = 0$ to $t = 1$ s, forward steady-state running for $1 \le t \le 3$ s, forward braking to reach zero speed within the interval from $3 \le t \le 4$ s, reverse acceleration from $t = 4$ to $t = 5$ s, reverse steady-state running for $5 \le t \le 7$ s, and reverse braking to reach zero speed within the interval from $7 \le t \le 8$ s.

The simulated and experimental responses of the proposed MRAC speed estimation SFOC IM drive with FTA stator resistance parameter identification under a 2 N-m load and a reversible steady-state speed command of 1600 rev/min for the first three running cycles are shown in Figs. 5 and 6, respectively. Here, the stator resistance was artificially increased by 30% at 12 s. Each figure contains six plots: (a) command (dashed line) and estimated (solid line) rotor speed values; (b) command (dashed line) and actual (solid) rotor speed values; (c) q-axis stator current; (d) electromagnetic torque; (e) identified stator resistance; and (f) estimated synchronous position angle.

Both the simulated and experimental responses under reversible transient and steady-state operating conditions show that the proposed MRAC scheme provides accurate rotor speed estimation. The responses of the q-axis stator current and electromagnetic torque effectively indicate the imposed load conditions. Furthermore, the incorporation of the FTA stator resistance parameter identification enhances the robustness of the MRAC speed estimation SFOC IM drive

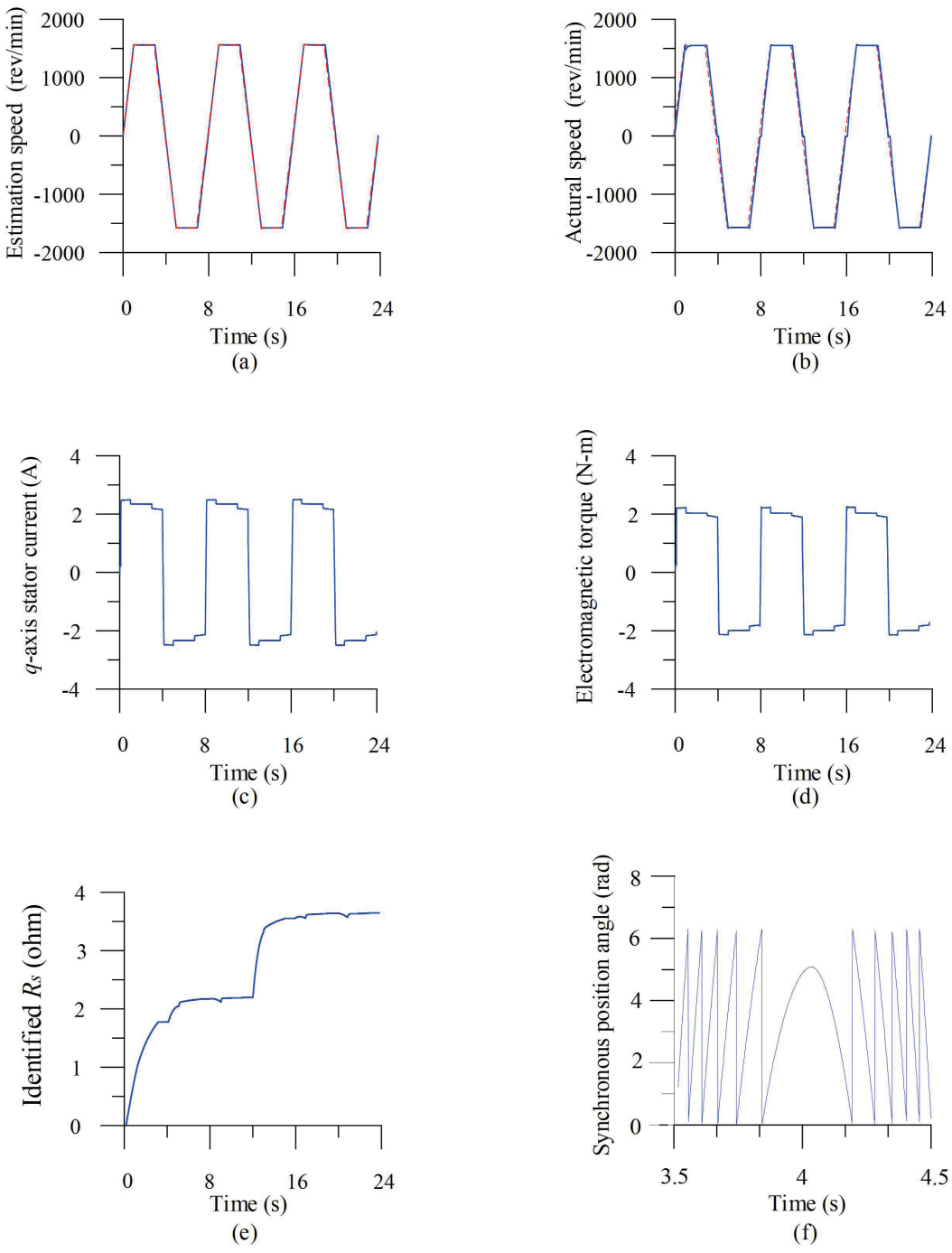

Fig. 5. (Color online) Simulated responses of the proposed MRAC speed estimation SFOC IM drive with FTA stator resistance parameter identification under a 2 N-m load and a reversible steady-state speed command of 1600 rev/min: (a) command (dashed line) and estimated (solid line) rotor speed values, (b) command (dashed line) and actual (solid) rotor speed values, (c) q-axis stator current, (d) electromagnetic torque, (e) identified stator resistance, and (f) estimated synchronous position angle.

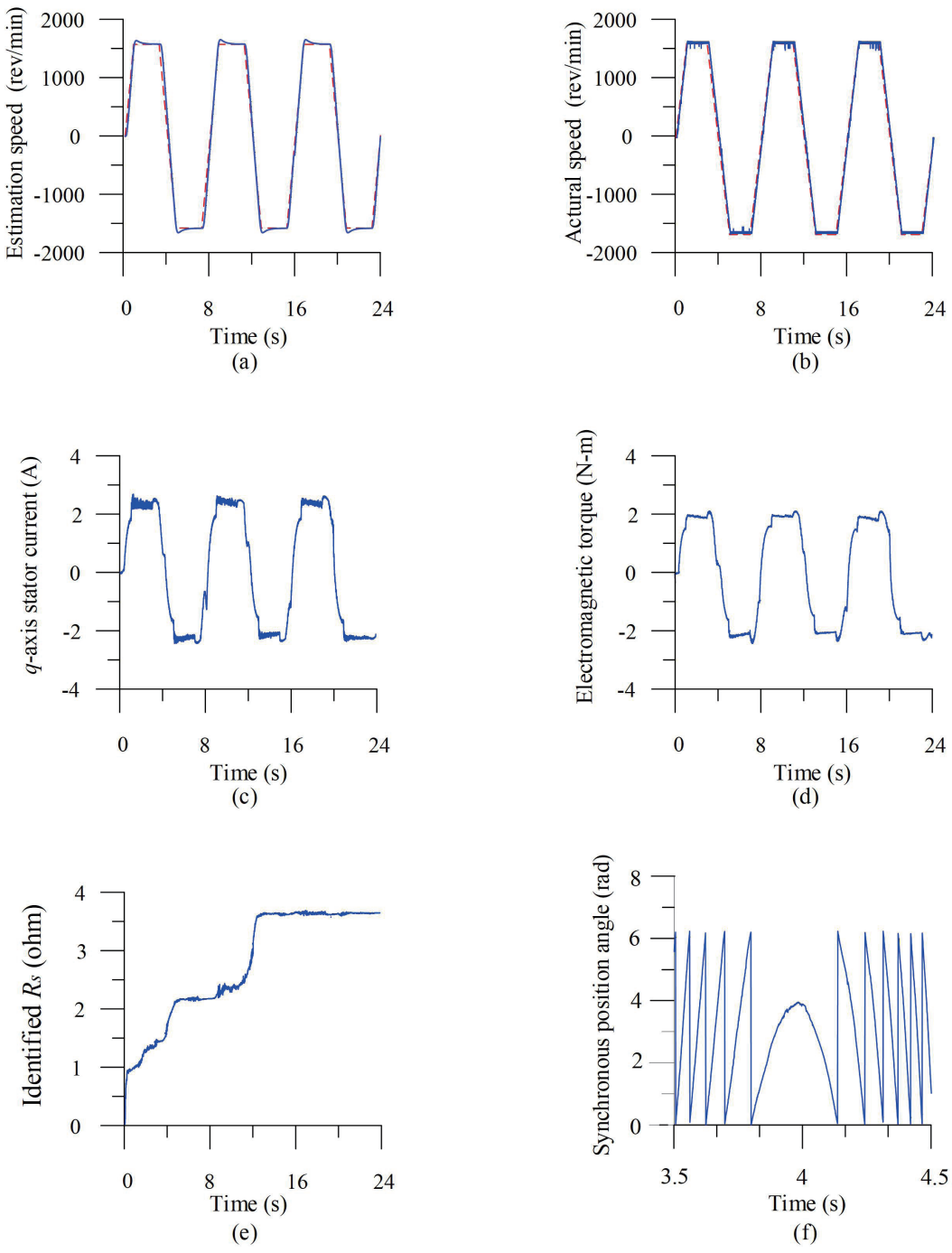

Fig. 6. (Color online) Experimental responses of the proposed MRAC speed estimation SFOC IM drive with FTA stator resistance parameter identification under a 2 N-m load and a reversible steady-state speed command of 1600 rev/min: (a) command (dashed line) and estimated (solid line) rotor speed values, (b) command (dashed line) and actual (solid) rotor speed values, (c) q-axis stator current, (d) electromagnetic torque, (e) identified stator resistance, and (f) estimated synchronous position angle.

against temperature-dependent variations in motor resistances. In addition, the sawtooth profile observed in the estimated synchronous position angle confirms the validity of the coordinate transformation between the three-phase reference frame and the two-axis synchronous reference frame. Consequently, the developed MRAC speed estimation SFOC IM drive with FTA stator resistance identification achieves the expected performance objectives.

6. Conclusions

An FTA stator resistance parameter identification scheme was developed for the MRAC speed estimation SFOC IM drive. The decoupled SFOC IM drive was formulated on the basis of stator current and flux. The speed, flux, and *d*-axis and *q*-axis stator current controllers were designed using root locus and Bode plot techniques. Rotor speed estimation was carried out according to MRAC theory by utilizing the motor's reactive power, whereas compensation for temperature-dependent resistance variations was achieved through the FTA online stator resistance identification approach. The three-phase stator currents required for implementing the MRAC speed estimation SFOC IM drive were measured using Hall-effect current sensors. Both simulated and experimental responses under reversible steady-state speed commands with load conditions verify the effectiveness and favorable performance of the proposed MRAC speed estimation SFOC IM drive incorporating FTA stator resistance parameter identification.

Acknowledgments

This study was supported by the National Science and Technology Council of Taiwan under contract number NSTC 114-2637-E-167-007 (duration: August 1, 2025–July 31, 2026).

References

1 Y. C. Luo, Z. J. Hu, W. Y. Wang, and W. C. Pu: Sens. Mater. **37** (2025) 3475. https://doi.org/10.18494/SAM.5529
2 G. Pellegrino, P. Guglielmi, E. Armando, and R. I. Bojoi: IEEE Trans. Ind. Appl. **46** (2010) 1416. https://doi.org/10.1109/TIA.2010.2049554
3 M. H. Holakooie and G. Iwanski: IEEE J. Emerging. Sel. Top. Power Electron. **9** (2021) 5452. https://doi.org/10.1109/JESTPE.2020.3042305
4 S. Foti, A. Testa, S. D. Caro, T. Scimone, and M. Pulvirenti: IEEE Trans. Ind. Appl. **55** (2019) 3759. https://doi.org/10.1109/TIA.2019.2906862
5 S. Yang, D. Ding, X. Li, Z. Xie, X. Zhang, and L. Chang: IEEE Trans. Energy Conv. **34** (2019) 1033. https://doi.org/10.1109/TEC.2018.2880796
6 J. Chen, J. Mei, X. Yuan, Y. Zuo, and C. H. T. Lee: IEEE Trans. Power Electron. **37** (2022) 14. https://doi.org/10.1109/TPEL.2021.3094583
7 M. Hinkkanen, L. Harnefors, and J. Luomi: IEEE Trans. Power Electron. **25** (2010) 1173. https://doi.org/10.1109/TPEL.2009.2039650
8 H. K. Khalil, E. G. Strangas, and S. Jurkovic: IEEE Trans. Cont. Sys. Tech. **17** (2009) 327. https://doi.org/10.1109/TCST.2008.2000977
9 M. Montanari, S. M. Peresada, C. Rossi, and A. Tilli: IEEE Trans. Cont. Sys. Tech. **15** (2007) 1049. https://doi.org/10.1109/TCST.2007.899714
10 S. Yang, D. Ding, X. Li, Z. Xie, X. Zhang, and L. Chang: IEEE Trans. Energy Conv. **32** (2017) 1562. https://doi.org/10.1109/TEC.2017.2699681
11 S. Nasri, S. Krim, H. Moussa, and M. F. Mimouni: Proc. 2025 IEEE Int. Advanced Systems and Emergent Technologies Conf. (IC_ASET, 2025) 1–6. https://doi.org/10.1109/IC_ASET65966.2025.11232277

12 M. Comanescu: Proc. 2022 Int. Power Electronics, Electrical Drives, Automation and Motion Sym. (SPEEDAM, 2022) 1–6. https://doi.org/10.1109/SPEEDAM53979.2022.9842179
13 S. A. A. Rizvi and M. B. Kadri: Proc. 2013 IEEE 9th Int. Emerging Technologies Conf. (ICET, 2013) 1–6. https://doi.org/10.1109/ICET.2013.6743522
14 Z. Boussada, M. B. Hamed, and L. Sbita: Proc. 2014 Int. Electrical Sciences and Technologies in Maghreb Conf. (CISTEM, 2014) 1–5. https://doi.org/10.1109/CISTEM.2014.7077071
15 H. Rehman and A. Khurram: Proc. 2017 IEEE Vehicle Power and Propulsion Conf. (VPPC, 2017) 1–5. https://doi.org/10.1109/VPPC.2017.8330885
16 D. Chen, W. Kong, R. Qu, and L. Zhou: IEEE Trans. Ind. Electron. **69** (2022) 4440. https://doi.org/10.1109/TIE.2021.3078402
17 J. Chen and J. Huang: IEEE Trans. Power. Electron. **32** (2017) 4587. https://doi.org/10.1109/TPEL.2016.2596839
18 J. Chen, J. Huang, and Y. Sun: IEEE Trans. Ind. Electron. **32** (2019) 2659. https://doi.org/10.1109/TIE.2018.2849964
19 G. Pellegrino, P. Guglielmi, E. Armando, and R. I. Bojoi: IEEE Trans. Ind. Appl. **46** (2010) 1416. https://doi.org/10.1109/TIA.2010.2049554
20 G. Pellegrino, R. I. Bojoi, P. Guglielmi, and F. Cupertino IEEE Trans. Ind. Appl. **46** (2010) 1970. https://doi.org/10.1109/TIA.2010.2057395
21 L. Zhao, J. Huang, J. Chen, and M. Ye: IEEE Trans. Power. Electron. **31** (2016) 6494. https://doi.org/10.1109/TPEL.2015.2504399
22 J. Chen, J. Huang, and Y. Sun: IEEE Trans. Ind. Electron. **66** (2019) 2659. https://doi.org/10.1109/TIE.2018.2849964
23 M. S. Morey, V. B. Virulkar, and G. A. Dhomane: Proc. 2016 Int. Emerging Trends in Electrical Electronics & Sustainable Energy Systems Conf. (ICETEESES, 2016) 179–185. https://doi.org/10.1109/ICETEESES.2016.7581381
24 J. Chen and J. Huang: IEEE Trans. Power. Electron. **32** (2017) 4587. https://doi.org/10.1109/TPEL.2016.2596839
25 J. Holtz: IEEE Trans. Ind. Electron. **53** (2006) 7. https://doi.org/10.1109/TIE.2005.862324
26 M. R. Hachicha, M. Ghariani, and R. Neji: Proc. 2014 Int. Electrical Sciences and Technologies in Maghreb Conf. (CISTEM, 2014) 1–11. https://doi.org/10.1109/CISTEM.2014.7077060
27 C. H. Liu: Control of AC Electrical Machines (Tunghua, Taipei, 2008) 4th ed., Chap. 6 (in Chinese).
28 Y. C. Luo, S. Y. Xie, C. H. Lin, and Y. P. Kuo: Sens. Mater. **35** (2023) 2101. https://doi.org/10.18494/SAM.4290
29 Y. C. Luo and Z. S. Ke: Smart. Science. **6** (2018) 363. https://doi.org/10.1080/23080477.2018.1451207